A Survey on Convex Image Denoising Methods

Hao Li Yi Zhang Sihan He Tianrui Wang

I. TEAM ASSIGNMENT

Tianrui Wang is responsible for introduction, conclusion and future works part. Hao Li is responsible for the state of the art method A, Sihan He is responsible for the state of the art method B, Yi Zhang is responsible for the state of the art method C. Hao Li, Sihan He and Yi Zhang together finish the statement of problem part.

II. INTRODUCTION

A. MOTIVATION

Digital images play an important role in our daily life, such as satellite television, computer resonance imaging, and in research and technology. Data sets collected by image sensors are contaminated with noise due to imperfect instrumentation, while disturbed natural phenomena can also degrade the quality of data of interest. On the other hand, the transmission and compression of images also introduce noise. Therefore, image denoising is a necessary and primary step in image analysis. It is necessary to employ some effective image denoising techniques to prevent this type of corruption in digital images.

B. PREVIOUS WORKS

A wide range of approaches have been proposed to provide supplementary information for estimating the denoised image. Depending on the image information used, the approaches can be categorized into internal (use solely the input noisy image) and external (use external images with or without noise) denoising methods. In addition, some work has shown that the combination or fusion of internal and external information can lead to better denoising performance. [1] The category of implicit methods adopt priors of high quality images implicitly, where the priors are embedded into specific restoration operations. Such an implicitly modeling strategy was used in most of the early image denoising algorithms. [2], [3] Based on the assumptions of high quality images, heuristic operations have been designed to generate estimations directly from the degraded images. For example, based on the smoothness assumption, filtering-based methods have been widely utilized to remove noise from noisy images. [4] Although the image prior is not explicitly modeled, the prior for high-quality images is considered when designing filters to estimate high-resolution images. Such implicitly modeling schemes have dominated the area of image denoising for decades. To generate the piece-wise smooth image signal, diffusion methods have been proposed to adaptively smooth image contents. By assuming that the wavelet coefficients of natural image are sparse, shrinkage methods have been developed to denoise images in wavelet domains. [5] Based on the observation that natural image contains many repetitive local patterns, the non-local mean filtering approach has been suggested to profile from the image non-local self-similarity (NSS) prior. [6] Although these simple heuristic operations have limited capacity in producing high-quality restoration results, these studies have greatly deepened researchers' understanding of natural image modeling. Many useful conclusions and principles are still applicable to modern image restoration algorithm design.

C. INTENDED CONTRIBUTIONS

We will first establish the problem by analyzing the three aspects of convex problem–primal, dual, KKT conditions and relate it to the image denoising topic. We will survey state-or-art image denoising methods in this paper. Then we will propose three state-of-art algorithms with different approaches.

Each paper has its own novelty. For the HSI paper, it converted denoising problem into a multi-objective optimization problem. This approach reflects the optimization and complementary capabilities of the multi-angle information contained in noisy hyperspectral remote sensing images. For the second paper,They defined a new transforms depended tensor rank and the cor- responding tensor nuclear norm. Then we solve the TR-PCA problem by convex optimization whose objective is a weighted combination of the new tensor nuclear norm and l1-norm.

For our work, firstly, we want to explore one algorithm - multi-objective low-rank and sparse image denoising framework that ensures effective optimization and can solve the problem of inaccurate sparse and unstable modeling results due to convex relaxation and sensitive regularization parameters when restoring clean hyperspectral images.

Secondly, we aim to review a general image denoising algorithm which recovers the underlying low-rank and sparse components with high probability and allows to use any invertible linear transforms.

Last but not least, in order to denoise images faster and more stable than curent gradient descent algorthms, we are employing Chambolle's Dual methods to minimize our image denosing objective.

D. ORGANIZATION OF THE PAPER

In this paper, we follow the format in the guideline. Our work is largely divided into four main sections. The first section is Statement of the problem. In this section, the problem is described in mathematical form, including its primal problem, the dual problem and the KKT conditions. Then, in the Intended Approaches section, different image denoising methods are surveyed in detail. The Conjectured

Results section describes and compares the results of various denoising methods. In the end, papers we surveyed are listed in the References section.

III. STATEMENT OF THE PROBLEM

A noised image f can be viewed as the sum of an unknown ideal image u and additive white Gaussian noise with mean 0 and variance σ^2. Therefore, we need to compute the unknown clean image u which satisfy the constraint,

$$\|u - f\|_2^2 \leq |\Omega|\sigma^2$$

To solve this problem, we can represent the constraint as minimize g(u), as:

$$\begin{aligned} \min_u \quad & g(u) \\ s.t. \quad & \|u - f\|_2^2 \leq |\Omega|\sigma^2 \ . \end{aligned}$$

Using Lagrange multiplier, it can be rewrote as:

$$\min_u \quad g(u) + \lambda(\ \|u - f\|_2^2 - |\Omega|\sigma^2\ )$$

There is a relation between λ and σ and λ is determined by σ. Therefore, once λ is known, the above problem can be rewrote as:

$$\min_u \quad g(u) + \lambda\ \|u - f\|_2^2$$

Then consider the constraint function g(u). Usually, the constrain is about the gradient of the image u, for example:

$$g(u) = \int_\Omega |\nabla_x u| dx$$

A. PRIMARY

After the above analysis, the primal problem of image denoting can be derived as :

$$\min_u \quad \int_\Omega |\nabla_x u|^2 dx + \lambda\ \|u - f\|_2^2$$

B. DUAL

The dual form can be wrote as:

$$\begin{aligned} \int_\Omega |\nabla_x u| &= \max_{\omega \in C_O^1(\Omega), |\omega| \leq 1} \quad \int_\Omega \nabla_x u \cdot\ \omega \\ &= \max_{|\omega| \leq 1} \quad \int_\Omega -u \operatorname{div} \omega \end{aligned}$$

Therefore, the dual problem of image denoting is:

$$\min_u \quad \max_{\omega \in C_O^1(\Omega), |\omega| \leq 1} \quad \int_\Omega -u \operatorname{div} \omega + \lambda\ \|u - f\|_2^2$$

With the help of min-max theorem, we can first

$$\min_{\omega \in C_O^1(\Omega), |\omega| \leq 1} \quad \frac{1}{2}\ \|\operatorname{div} \omega + 2\,\lambda f\|_2^2$$

Then, compute u as $u = f + \frac{1}{2\lambda}$

C. KKT CONDITIONS

According to the defnition of Karush-Kuhn-Tucker Condition of the problem are as follows:

$$\begin{gathered} \nabla_u \mathrm{L} = \nabla \mathrm{g(u)} + \lambda \nabla(\|u - f\|_2^2 - |\Omega|\sigma^2\ ) = 0 \\ \|u - f\|_2^2 - |\Omega|\sigma^2 \leq 0 \\ \lambda \geq 0 \\ \lambda(\ \|u - f\|_2^2 - |\Omega|\sigma^2\ ) = 0 \end{gathered}$$

IV. STATE-OF-THE-ART METHODS

In this section, we will investigate into three state of the art convex optimization approaches on image denoising.

A. *Multi-Objective Low-Rank and Sparse Model for Hyperspectral Image Denoising*

Due to the inevitable existence of Gaussian noise and sparse in the process of data representation, the quality and applications of hyperspectral images (HSIs) is degraded and limited. Traditionally, low-rank and sparse matrix decomposition methods are usually leveraged for clean HSIs restoration. However, the optimization of the l_0-norm for the sparse modeling is a non-convex and NP-hard problem. Convex relaxation and regulation parameters, which are usually used for optimizing the l_0-norm for spare modeling, could often lead to inaccurate results. In order to address the issue, an accurate multi-objective low-rank and sparse denoising framework [7] was proposed for accurate HSIs denoising. It modeled l_0-norm as sparse noise, and optimized it with an evolutionary algorithm. Therefore, this image denoising problem could be converted into the problem of multi-objective optimization with the data fidelity term, the sparse term, and low-rank term optimized simultaneously, without sensitive regularization parameters.

1) INTENDED APPROACHES: The overall framework of the proposed accurate multi-objective low-rank and sparse model (AMOLRS) is shown as Fig. 1, which mainly involves three stages: Preprocessing for the HSI, Multi-Objective Modeling for AMOLRS, and Model Optimization for AMOLRS.

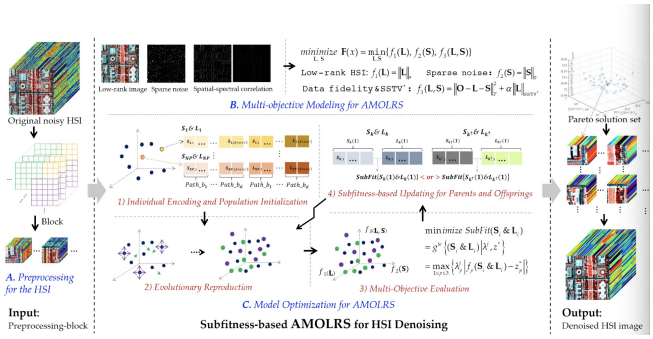

Fig. 1. The basic framework of AMOLRS. [7]

a) Preprocessing for the HSI: For HSIs denoising, the sparse noise image matrices and low-rank clean HSI are first encoded into the solution individuals, which then form a population to execute the evolutionary operations. In order to solve the problem that the length of the solution and the search space may be too large to be optimized and searched, a block-based preprocessing is applied, which is shown as Fig.2. We can see, the original size of the cube is $c \times r \times d$, and the size after processing is $u \times u' \times d$.

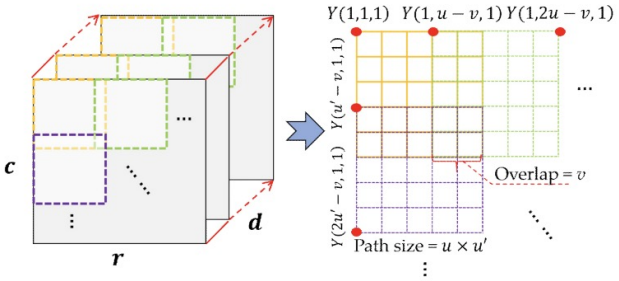

Fig. 2. The block-based preprocessing. [7]

b) Multi-Objective Modeling for AMOLRS : Since a set of trade-off solutions can be generated by the multi-objective evolutionary algorithms (MOEA) for balancing the multiple objective functions, and the MOEA is also able to deal with the NP-hard and non-convex problem [8]. Thus, MOEA can be introduced to solve the low-rank and sparse image denoising of HSIs problems. By introducing MOEA, the l_0-norm for sparse noise could be considered, and the sensitive weight parameters don't need to be preset manually. Therefore, we can represent this problem of image denoising as:

Where $\|O - L - S\|_F^2$ is the data fidelity term, and α is a weight to balance the SSTV terms and data fidelity.

c) Model Optimization for AMOLRS: The first step is for the individual encoding and population initialization. For the individual encoding part, the low-rank cube matrix and sparse noise cube matrix both get encoded in an individual for one path cube from the original HSI cube. For the initial values of the individual, the TV/l2-norm method [9] is applied to obtain low-rank image matrix and initial sparse noise

$$\underset{\mathbf{L},\,\mathbf{S}}{minimize}\ \mathbf{F}(x) = \min_{\mathbf{L},\mathbf{S}}\{f_1(\mathbf{L}),\, f_2(\mathbf{S}),\, f_3(\mathbf{L},\mathbf{S})\}$$

$$\begin{cases} \text{Low-rank HSI: } f_1(\mathbf{L}) = \|\mathbf{L}\|_* \\ \text{Sparse noise: } f_2(\mathbf{S}) = \|\mathbf{S}\|_0 \\ \text{Data fidelity\&SSTV}^{\dagger}\text{:} \\ f_3(\mathbf{L},\mathbf{S}) = \|\mathbf{O}-\mathbf{L}-\mathbf{S}\|_F^2 + \alpha\|\mathbf{L}\|_{\text{SSTV}^{\dagger}} \end{cases}$$

image matrix. A population means a solution set, where NP individuals are constructed, in which one individual is a vector representation for the sparse noise and low-rank clean images from the noisy HSIs. The population initialization could be represented as: where $\{S_i \& L_i\}$' is the result from TV/l2-

$$\underset{\mathbf{L}}{minimize}\ \ \frac{\Theta}{2}\times\|\mathbf{O}-\mathbf{L}\|_F^2 + \|\mathbf{L}\|_{\text{SSTV}} \tag{10}$$

$$\{\mathbf{S}_i \,\&\, \mathbf{L}_i\} = \begin{cases} N\left(\{\bar{\mathbf{S}}_i \,\&\, \bar{\mathbf{L}}_i\}', \delta^2\right) & if\ rand(0,1) < \xi \\ \{\mathbf{S}_i \,\&\, \mathbf{L}_i\}' & otherwise \end{cases} \tag{11}$$

norm method, $\{S_i \& L_i\}$ is the initialized individuals $\{\bar{S}_i \& \bar{L}_i\}$' is the mean value, δ is the standard deviation, and ξ is 0.5. Then Evolutionary Reproduction is utilized for individual reproduction in the population. Due to the complexity of for the optimization of multi-objective denoising, a Gaussian local search process and the DE algorithm are employed. To search for the "promising regions" in the image, solutions with good fitness are considered to be located after the long-distance rough search, and the most promising can be then found through region local search by a short-distance search. The process can be represented as:

$$\{\mathbf{S}_{i,j} \,\&\, \mathbf{L}_{i,j}\}^{\Omega} = \begin{cases} \{\mathbf{S}_{i,j} \,\&\, \mathbf{L}_{i,j}\}^{de} & if\ \left(rand(0,1) \le CR\ or\ j = j^{rand}\right) \\ \{\mathbf{S}_{i,i} \,\&\, \mathbf{L}_{i,j}\} & otherwise \end{cases}$$

$$\{\mathbf{S}_{i,j} \,\&\, \mathbf{L}_{i,j}\}^{de} = \{\mathbf{S} \,\&\, \mathbf{L}\}_{r1} + F \times \left(\{\mathbf{S} \,\&\, \mathbf{L}\}_{r2} - \{\mathbf{S} \,\&\, \mathbf{L}\}_{r3}\right)$$

where CR∈[0,1] is crossover rate, j^{rand} is randomly selected from 1 to $2 \times d \times u \times u$, F is a factor for scaling, $\{S\&L\}_{r1}$, $\{S\&L\}_{r2}$, and $\{S\&L\}_{r3}$ are three random individuals, and $\{S_{i,j}\&L_{i,j}\}^{\Omega}$ is a new individual.

In order to reduce the length of the individual, a subfitness-based individual evaluation and updating strategy is leveraged for the multi-objective denoising. To get the SSTV term, the horizontal TV (HTV) and vertical TV (VTV) are calculated. Therefore, the $SSTV^{+}$ can be representd as: Subsequently,

$$\|\mathbf{L}\|_{\mathrm{SSTV}^{\dagger}} = \|\mathbf{L}_k(q)\|_{\mathrm{HTV}} + \|\mathbf{L}_k\|_{\mathrm{VTV}}$$

$$SubFit(\mathbf{S}_i \,\&\, \mathbf{L}_i) = g^{te}\left\{(\mathbf{S}_i \,\&\, \mathbf{L}_i)\middle|\lambda^j, z^*\right\} = \max_{1\le p\le 3}\left\{\lambda_p^j \middle| f_p(\mathbf{S}_i \,\&\, \mathbf{L}_i) - z_p^*\right\}$$

$$s.t.\ \left[\begin{array}{l} \lambda_p^j \ge 0;\ \sum_{p=1}^{3}\lambda_p^j = 1;\ z^* = (z_1^*, z_2^*, z_3^*)^T; \\ z_p^* = \min\left\{f_p(\mathbf{S}_i \,\&\, \mathbf{L}_i)\middle|(\mathbf{S}_i \,\&\, \mathbf{L}_i) \in \Omega\right\} \end{array}\right]$$

multi-objective evaluation and population should be updated based on the subfitness. The updating process is as follows: First, parent individual and offerspring individual are separately denoted as: $S_k \& L_k$ and $S_k^+ \& L_k^+$. For each band, d subsitness are calculated. $SubFit\{S_k(i) \& L_k(i)\}$ is the subcomponent between $S_k(i) \& L_k(i)$. After comparing all the subcomponents, the new individual can be obtained as:

$$\{\mathbf{S}_{k^*}(i) \,\&\, \mathbf{L}_{k^*}(i)\} = \begin{cases} \{\mathbf{S}_{k^{\dagger}}(i) \,\&\, \mathbf{L}_{k^{\dagger}}(i)\} \\ if\ SubFit\{\mathbf{S}_k(i) \,\&\, \mathbf{L}_k(i)\} > SubFit\{\mathbf{S}_{k^{\dagger}}(i) \,\&\, \mathbf{L}_{k^{\dagger}}(i)\} \\ \{\mathbf{S}_k(i) \,\&\, \mathbf{L}_k(i)\} \qquad otherwise \quad i = 1, 2, ..., d \end{cases}$$

Finally, all the above steps are repeated until the number of generations is less or equals to the maximum number of generations. The stopping conditions are listed as follows:

2) CONJECTURED RESULTS: To verify the performance of the proposed approach, seven traditional and advanced methods was compared: the TV/l2-norm method [9], the BM4D method [10], the LRMR method [11], the LRTV method [12], the SSTV method [13], a fast hyperspectral image denoising and inpainting method based on low-rank and sparse representation (FastHyDe) [14], a TV regularized low-rank tensor decomposition method (LRTDTV) [15], a subspace-based nonlocal low-rank and sparse factorization method (SNLRSF) [16], a mixed Gaussian and sparse noise reduction method (HyMiNoR) [17], and the LLRSSTV method [18]. Besides, l_1 norm was also used for sparse modeling as comparison method to prove the effectiveness of using the l0 norm for accurate sparse noise modeling. The comparison results are shown in Fig.3. We can see from the figure that the proposed method achieved the best overall performance compared to all other methods in terms of most metrics.

Case1-1	**To all bands:** Gaussian noise with signal-to-noise ratio (SNR) equal to 10dB; impulse noise with density equal to 0.05.
Case1-2	**To all bands:** Gaussian noise with SNR equal to 5dB; impulse noise with density equal to 0.05.
Case1-3 /4/5/6	**To all bands:** Gaussian noise with SNR equal to 10, 30, 40, and 50dB; impulse noise with density equal to 1.
Case1-7	**Different variance** zero-mean Gaussian noise is added to all bands, with the variance value being **randomly selected** from 0 to 0.05.
Case 2	**To all bands:** Impulse noise with density equal to 0.05. **To bands 17, 27, 60, 100, 150** stripe noise (rate = 0.2, mean = 0.2).
Case 3	**To all bands:** Gaussian noise with SNR equal to 10dB; impulse noise with density equal to 0.05. **To bands 17, 27, 60, 100, 150** stripe noise (rate = 0.2, mean = 0.2).
Case 4	**To all bands:** Gaussian noise with SNR equal to 10dB; impulse noise with density equal to 0.05. **To bands 17, 27, 60, 100, 150** stripe noise (rate = 0.2, mean = 0.2). Dead lines (row number = 100, 101, 110, 150, 160; column number = 50, 109, 110, 111, 120, 130)
Case 5	**Different variance** zero-mean Gaussian noise is added to all bands, with the variance value being **randomly selected** from 0 to 0.05. **To bands 17, 27, 60, 100, 150** stripe noise (rate = 0.2, mean = 0.2). Dead lines (row number = 100, 101, 110, 150, 160; column number = 50, 109, 110, 111, 120, 130)

B. Transforms based Tensor Robust PCA

Motivated by the linear transforms based tensor-tensor product and tensor SVD, Canyi Lu [19] proposed a transforms based tensor robust PCA fromework to solve the corrupted low-rank tensors recovery problem through convex optimization. First, a new transforms depended tensor rank and corresponding tensor nuclear norm is defined. When the invertible linear transform can meet the requirement of: $L^T L = LL^T$. Subsequently, the Tensor Robust Principal Component Analysis (TRPCA) problem is solved with convex optimization whose objective is a weighted combination of the new tensor nuclear norm and l_1-norm, as follows: $\min_{L,\varepsilon}\langle L\rangle_* + \lambda\langle S\rangle_1, s.t. X = L + S$.Compared to traditional methods, this new TRPCA problem is more general for supporting any invertible linear transforms.

1) INTENDED APPROACHES: First, it defines new tensor nuclear norm which is induced by the t-product under linear transforms. T-product equals to the matrix-matrix product under the discrete Fourier transform. Then the frontal-slice-wise product is defined as $R = P \odot Q$. Let $\bar{A} = A_{X3}F_{n3}$. where F_{n3} means the Discrete Fourier Transform (DFT) matrix, and $X3$ represents the mode-3 product. We define $/barA$ as:

where bdiag is an operator mapping. Let $B \in R^{n2\times l\times n3}$, and $A \in R^{n1\times n2\times n3}$. Therefore we can get the t-product as:

THE QUANTITATIVE RESULTS OF THE DIFFERENT DENOISING METHODS IN THE SIMULATED DATA EXPERIMENTS

#	Index	Noisy	M1	M2	M3	M4	M5	M6	M7	M8	M9	M10	M11	M12
1-1	MPSNR↑	13.81	22.04	23.77	26.06	27.39	27.17	25.82	24.32	25.74	25.18	28.74	28.79	**29.08**
	MSSIM↑	0.5321	0.8545	0.8935	0.9282	0.9524	0.9414	0.9444	0.9129	0.9444	0.9353	0.9577	0.9592	**0.9615**
	MFSIM↑	0.7703	0.9036	0.9207	0.9393	0.9603	0.9530	0.9570	0.9370	0.9550	0.9512	0.9638	0.9644	**0.9662**
	ERGAS↓	417.46	162.24	133.00	102.53	88.58	90.95	105.21	124.88	106.34	113.65	75.99	75.62	**73.66**
	MSAM↓	0.4580	0.1850	0.1508	0.1089	0.1283	0.1271	0.1247	0.1362	0.1288	0.1370	0.1087	0.1067	**0.1060**
1-2	MPSNR↑	10.92	18.46	20.09	23.09	24.43	23.45	21.50	20.88	21.55	21.06	25.10	25.19	**26.07**
	MSSIM↑	0.3610	0.7294	0.7997	0.8693	0.9144	0.8829	0.8885	0.8542	0.8874	0.8748	0.9144	0.9170	**0.9309**
	MFSIM↑	0.6912	0.8544	0.8704	0.8994	0.9384	0.9187	0.9258	0.9049	0.9200	0.9174	0.9373	0.9348	**0.9464**
	ERGAS↓	581.90	244.45	202.85	143.73	123.82	138.50	172.41	185.12	171.50	181.58	114.64	113.41	**102.96**
	MSAM↓	0.5710	0.2516	0.1894	0.1335	0.1602	0.1757	0.1654	0.1728	0.1664	0.1786	0.1491	0.1455	0.1337
1-3	MPSNR↑	12.43	20.37	22.20	25.61	27.05	26.80	23.89	22.87	23.95	23.39	28.37	27.96	**28.79**
	MSSIM↑	0.4581	0.8032	0.8612	0.9229	0.9489	0.9371	0.9246	0.8925	0.9259	0.9141	0.9543	0.9559	**0.9590**
	MFSIM↑	0.7393	0.8814	0.9031	0.9336	0.9579	0.9498	0.9450	0.9250	0.9436	0.9379	0.9615	0.9608	**0.9643**
	ERGAS↓	489.34	196.42	159.10	107.80	92.14	94.75	131.29	147.48	130.32	139.18	79.25	82.82	**76.05**
	MSAM↓	0.5098	0.2145	0.1662	0.1115	0.1320	0.1313	0.1417	0.1508	0.1430	0.1528	0.1124	**0.1077**	0.1085
1-4	MPSNR↑	14.69	22.64	24.30	33.38	33.38	34.66	27.31	27.76	27.55	26.57	36.27	36.10	**36.61**
	MSSIM↑	0.6112	0.8664	0.8979	0.9849	0.9859	0.9848	0.9567	0.9518	0.9596	0.9484	0.9909	0.9908	**0.9915**
	MFSIM↑	0.8505	0.9120	0.9295	0.9845	0.9861	0.9853	0.9654	0.9654	0.9681	0.9589	0.9902	0.9899	**0.9905**
	ERGAS↓	376.94	151.51	125.02	46.27	45.23	42.90	88.99	84.48	87.03	97.23	33.94	34.48	**32.59**
	MSAM↓	0.4212	0.1754	0.1525	0.0797	0.0632	0.0752	0.1098	0.0911	0.1122	0.1225	0.0602	0.0599	**0.0583**
1-5	MPSNR↑	14.72	22.65	24.20	33.59	33.94	35.04	27.35	27.83	27.62	26.61	36.77	36.60	**37.16**
	MSSIM↑	0.6132	0.8665	0.8963	0.9856	0.9877	0.9856	0.9570	0.9526	0.9600	0.9486	0.9916	0.9915	**0.9922**
	MFSIM↑	0.8564	0.9124	0.9289	0.9850	0.9882	0.9860	0.9653	0.9661	0.9681	0.9591	0.9908	0.9906	**0.9912**
	ERGAS↓	376.03	151.31	126.47	45.25	42.77	41.50	88.53	83.82	86.47	96.85	32.62	32.95	**31.18**
	MSAM↓	0.4200	0.1748	0.1539	0.0775	0.0669	0.0733	0.1088	0.0905	0.1114	0.1215	0.0583	0.0587	**0.0568**
1-6	MPSNR↑	14.72	22.66	24.14	33.62	34.00	35.08	27.36	27.84	27.64	26.56	37.22	36.61	**37.24**
	MSSIM↑	0.6134	0.8668	0.8949	0.9856	0.9879	0.9857	0.9572	0.9527	0.9601	0.9486	0.9922	0.9913	**0.9925**
	MFSIM↑	0.8569	0.9124	0.9283	0.9850	0.9884	0.9861	0.9654	0.9661	0.9683	0.9589	0.9913	0.9907	**0.9917**
	ERGAS↓	375.83	151.16	127.37	45.14	42.53	41.34	88.49	83.74	86.31	97.37	31.05	33.22	**30.09**
	MSAM↓	0.4203	0.1749	0.1547	0.0771	0.0606	0.0731	0.1089	0.0904	0.1115	0.1222	**0.0567**	0.0592	**0.0567**
1-7	MPSNR↑	18.31	25.04	27.03	27.68	29.09	29.09	30.63	25.90	27.71	30.28	30.67	30.68	**30.90**
	MSSIM↑	0.7011	0.9180	0.9414	0.9473	0.9661	0.9589	0.9760	0.9244	0.9501	0.9731	0.9712	0.9738	**0.9762**
	MFSIM↑	0.8387	0.9276	0.9512	0.9540	0.9699	0.9649	**0.9794**	0.9436	0.9550	0.9778	0.9738	0.9755	0.9781
	ERGAS↓	272.88	115.80	92.43	86.40	73.57	75.41	63.14	104.42	86.30	65.46	61.73	61.50	**60.84**
	MSAM↓	0.3486	0.1408	0.1230	0.1022	0.1134	0.1136	0.0958	0.1086	0.1012	0.0992	0.0940	**0.0902**	0.0962
2	MPSNR↑	17.69	24.96	23.47	32.12	33.79	34.54	30.31	27.02	30.15	29.84	36.33	36.33	**37.32**
	MSSIM↑	0.7591	0.9125	0.8938	0.9823	0.9861	0.9858	0.9704	0.9423	0.9738	0.9687	0.9875	0.9874	**0.9906**
	MFSIM↑	0.9191	0.9328	0.9450	0.9833	0.9852	0.9858	0.9729	0.9559	0.9761	0.9710	0.9881	0.9881	**0.9907**
	ERGAS↓	267.10	116.31	137.57	53.19	44.44	42.74	65.28	95.53	65.38	67.71	36.18	36.86	**32.02**
	MSAM↓	0.3243	0.1410	0.1797	0.0782	0.0759	0.0760	0.0977	0.1098	0.0956	0.0984	0.0734	0.0735	**0.0593**
3	MPSNR↑	13.79	22.04	23.75	25.84	27.36	27.14	25.64	24.22	25.50	25.17	28.69	28.67	**29.05**
	MSSIM↑	0.5313	0.8545	0.8934	0.9267	0.9520	0.9414	0.9404	0.9104	0.9410	0.9348	0.9556	0.9595	**0.9613**
	MFSIM↑	0.7697	0.9034	0.9202	0.9361	0.9600	0.9525	0.9543	0.9354	0.9525	0.9508	0.9623	0.9645	**0.9659**
	ERGAS↓	418.40	162.35	133.32	105.06	88.98	91.31	108.33	126.66	109.70	113.78	77.48	77.19	**73.99**
	MSAM↓	0.4588	0.1853	0.1513	0.1124	0.1288	0.1276	0.1314	0.1397	0.1351	0.1372	0.1142	0.1090	**0.1066**
4	MPSNR↑	13.75	21.98	23.59	25.59	27.29	27.08	25.51	24.11	25.29	25.17	28.56	28.58	**29.00**
	MSSIM↑	0.5302	0.8529	0.8908	0.9215	0.9516	0.9408	0.9372	0.9078	0.9365	0.9347	0.9529	0.9541	**0.9610**
	MFSIM↑	0.7688	0.9029	0.9190	0.9324	0.9597	0.9525	0.9530	0.9342	0.9503	0.9508	0.9607	0.9612	**0.9658**
	ERGAS↓	420.32	163.51	136.64	110.47	89.85	91.85	112.11	130.01	114.62	113.81	81.54	81.18	**74.48**
	MSAM↓	0.4605	0.1859	0.1542	0.1237	0.1296	0.1280	0.1371	0.1443	0.1422	0.1372	0.1209	0.1182	**0.1072**
5	MPSNR↑	17.91	24.89	26.65	28.84	27.29	28.74	29.84	25.64	29.55	29.85	30.20	29.99	**30.40**
	MSSIM↑	0.6918	0.9157	0.9396	0.9642	0.9409	0.9559	0.9667	0.9202	0.9655	0.9704	0.9671	0.9620	**0.9700**
	MFSIM↑	0.8336	0.9272	0.9481	0.9688	0.9499	0.9631	**0.9737**	0.9409	0.9708	0.9758	0.9692	0.9678	0.9729
	ERGAS↓	280.74	117.69	98.14	75.86	92.66	78.16	72.47	108.74	74.67	68.01	69.26	70.93	**64.54**
	MSAM↓	0.3534	0.1419	0.1275	0.1157	0.1122	0.1158	0.1103	0.1143	0.1172	0.1003	0.1090	0.1119	**0.0977**
	Time (s)↓		17.7	352.3	114.9	63.5	302.3	**2.3**	255.5	390.5	52.3	218.4	1028.3	929.3

M1: TV/L2. M2: BM4D. M3: LRMR. M4: LRTV. M5: SSTV. M6: FastHyDe. M7: LRTDTV. M8: SNLRSF. M9: HyMiNoR. M10: LLRSSTV. M11: MO/L1. M12: AMOLRS.

Fig. 3. Comparison results [7]

$$\mathcal{C} = \mathcal{A} * \mathcal{B} \Leftrightarrow \bar{\mathcal{C}} = \bar{\mathcal{A}} \odot \bar{\mathcal{B}} \Leftrightarrow \bar{C} = \bar{A}\bar{B}.$$

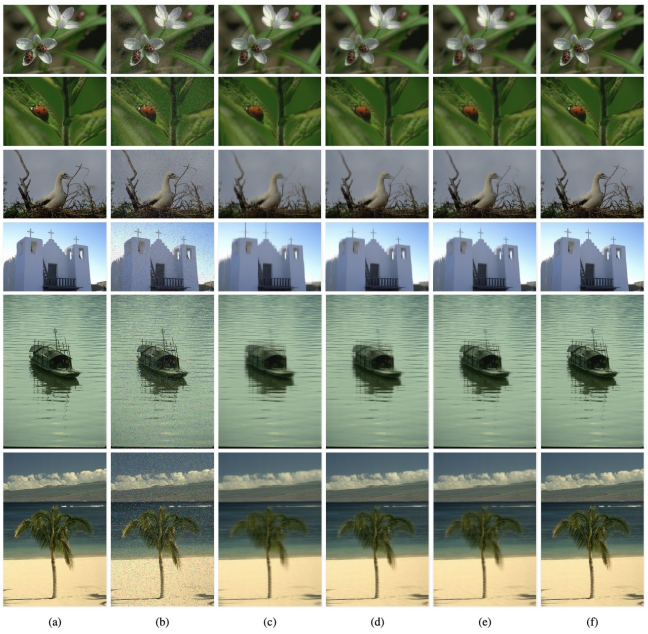

Fig. 4. Performance comparison for image recovery on some sample images. (a) Original image; (b) observed image; (c)-(f) recovered images by RPCA, SNN, TRPCA, and our TRPCA-DCT, respectively [19]

$$\bar{\boldsymbol{A}} = \texttt{bdiag}(\bar{\mathcal{A}}) = \begin{bmatrix} \bar{\boldsymbol{A}}^{(1)} & & & \\ & \bar{\boldsymbol{A}}^{(2)} & & \\ & & \ddots & \\ & & & \bar{\boldsymbol{A}}^{(n_3)} \end{bmatrix}$$

A more general definition of t-product is proposed utilizing any invertible linear transform for this discrete Fourier transform. In this work, the linear transform is considered as: $L : R^{n1\times n2\times n3} -> R^{n1\times n2\times n3}$.

Subsequently, the convex tensor nuclear norm is defined by inducing the t-product under L. First, assumption on L is given as: $L^T L = LL^T = lI_{n3}$, where l ¿ 0. Then, $\langle A, B\rangle = \frac{1}{l}\langle \bar{A}, \bar{B}\rangle$. $\|A\|_F = \frac{1}{\sqrt{l}}\|\bar{A}\|_F$

Therefore,the definition can be reached that for L be an invertible linear transform, and $A = u_{*L}S_{*L}v^T$ be the t-SVD of A, then the tensor nuclear norm of A under L can be represented as: $\|A\|_* := \langle S, I\rangle = \frac{1}{l}\langle \bar{A}\rangle_*$.

2) Conjectured results: we can format any color image of size $n_1 \times n_2$ to a tensor $n_1 \times n_2 \times n_3 \times n_4$, and $n_3 = 3$. 100 color images are randomly selected from the Berkeley segmentation dataset [20]. 10% of pixels is set to random values between 0 and 255. Three comparison models are utilized, the RPCA [21], SNN [22] and TRPCA [23]. In this experiment, DCT and ROM are used as the transforms in the new TRPCA method, which is defined as TRPCADCT and TRPCA-ROM, respectively. The Peak Signal-toNoise Ratio (PSNR) value [23] is used to evaluate the recovery performance. As can be seen from Fig. 4, the proposed TRPCA-DCT has achieved the best performance compared to all other comparison methods.

C. Chambolle's Dual Method

Inspired by the concept of total variation [24], Antonin Chambolle came up with a dual method which is faster to minimize the total variation [25], and performs better in its application of image denosing.

As we have described in the Statement of the Problem, the constraint function is usually expressed as the gradient of image, then the gradient will be ∇u, whose expression is below:

$$(\nabla u)_{i,j} = ((\nabla u)^1_{i,j}, (\nabla u)^2_{i,j}),$$

for i, j = 1,2,3,$\cdots$, N.

The discrete total variation will be:

$$J(u) = \sum_{1\le i,j\le N} |(\nabla u)_{i,j}|,$$

where $|(\nabla u)_{i,j}| = \sqrt{((\nabla u)^1_{i,j})^2 + ((\nabla u)^2_{i,j})^2}$.

With the help of divergence theorem $\nabla\cdot(fv)$ = $(\nabla f)\cdot v + f(\nabla\cdot v)$, we can rewrite J(u) as follows:

$$
\begin{aligned}
J(u) &= \sup\Big\{\int_\Omega u(x)\mathrm{div}\xi(x)dx\Big\} \\
&= \sup\Big\{\int_\Omega \mathrm{div}(u(x)\xi(x))dx - \int_\Omega (\nabla u(x))\cdot\xi(x)dx\Big\} \\
&= \sup\Big\{\int_{\partial\Omega} u(x)\xi(x)\cdot\hat{n}ds - \int_\Omega (\nabla u(x))\cdot\xi(x)dx\Big\} \\
&= \sup\Big\{-\int_\Omega (\nabla u(x))\cdot\xi(x)dx\Big\} \\
&= \int_\Omega |\nabla u|dx,
\end{aligned}
$$

where the second equality to last comes from the fact that is compact support, which means that is zero outside a compact set. Since J is one-homogeneous, the dual problem of J(u) is:

$$J^*(v) = \sup_u \langle u, v\rangle_{\mathbb{R}^{N\times N}} - J(u),$$

1) INTENDED APPROACHES:

a) Chambolle's projection algorithm with fixed λ: Chambolle proposed the algorithm to solve:

$$\min_{u\in\mathbb{R}^{N\times N}} \frac{\|u-g\|^2}{2\lambda} + J(u),$$

given $g \in R^{N\times N}$ and $\lambda > 0$. The Euclidean norm $\|\cdot\|$ is given by $\|\|^2 = \sum_{i,j=1}^N u_{i,j}^2$.

Its first order optimality condition satisfies

$$0 \in u - g + \lambda\partial J(u),$$

where $\partial J(u)$ is the subdifferential of J(u).

Then we have:

$$\frac{g-u}{\lambda} \in \partial J(u).$$

Using the convex optimization properties, we have $u \in \partial J(\frac{g-u}{\lambda})$, therefore we have:

$$0 \in \frac{(g-u)-g}{\lambda} + \frac{1}{\lambda}\partial J^*(\frac{g-u}{\lambda}),$$

This implies that $w = \frac{g-u}{\lambda}$ is the minimizer of

$$\frac{\|w - \frac{g}{\lambda}\|^2}{2} + \frac{1}{\lambda}J^*(w),$$

Therefore, the initial minimization problem can be reduced to solve for $\prod_K \frac{g}{\lambda}$. Since $\lambda > 0$, the minimizer w is also the minimizer of

$$\frac{\|\lambda w - g\|^2}{2\lambda} + J^*(w),$$

This means that we can solve for $\prod_{\lambda K} g$ to get the solution, and $u^* = g - \prod_{\lambda K} g$.

Since the closed convex set K is given by:

$\{\mathrm{div}\, p : p \in \mathbb{R}^{N\times N} \times \mathbb{R}^{N\times N}, |p_{i,j}| \le 1\}$

therefore, calculating $\prod_{\lambda K} g$ is equivalent to solve:

$$\min\{\|\lambda \mathrm{div}\, p - g\|^2 : p \in \mathbb{R}^{N\times N} \times \mathbb{R}^{N\times N}, |p_{i,j}|^2 \le 1\}$$

The KKT conditions satisfy

$$
\begin{aligned}
\big(\nabla(\lambda \mathrm{div} p - g)\big)_{i,j} + \alpha_{i,j}p_{i,j} &= 0 \\
\alpha_{i,j}(|p_{i,j}|^2 - 1) &= 0 \\
\alpha_{i.j} &\ge 0 \\
|p_{i,j}|^2 - 1 &\le 0.
\end{aligned}
$$

After analysing the above expressions and conditions, Chambolle's algorihtm with fixed λ can be expressed as follows:

Choose $\tau > 0$, and let inital value $p^0 = (0, 0)$, where 0 is an N by N zero matrix, and then

$$p_{i,j}^{n+1} = \frac{p_{i,j}^n + \tau(\nabla(\mathrm{div}p^n - \frac{g}{\lambda}))_{i,j}}{1 + \tau|(\nabla(\mathrm{div}p^n - \frac{g}{\lambda}))_{i,j}|}.$$

b) Chambolle's projection method with optimal λ: With the assumption that observed image g is the addition of a random Gaussian noise with variance σ^2 and an image u with little oscillation, Chambolle changed the optimization problem as:

$$\min\{J(u) : \|u-g\|^2 = N^2\sigma^2\}.$$

Chambolle choose λ_0 arbitrarily, and let $v_0 = \lambda_0 \mathrm{div}p$, where p is computed with the first Chambolle fixed λ algorithm. Suppose the input $\lambda = \lambda_0$, and $f_0 = \|v_0\|$, then for any $n \ge 0$, the iteration algorithm can be described as follows:

$$
\begin{aligned}
\lambda_{n-1} &= (\frac{N\sigma}{f_n})\lambda_n \\
v_{n+1} &= \lambda_{n+1}\mathrm{div}p \\
f_{n+1} &= \|v_{n+1}\|
\end{aligned}
$$

we can get the output $u = g - \lambda \mathrm{div}p$ if $\|f_{n+1}\ N^2\sigma^2\| \le$ tolenrance. During each iteration, p is computed with the first Chambolle fixed λ algorithm.

2) CONJECTURED RESULTS: The first group(Fig.5) of images show the results of the Chambolle's projection algorithm with fixed λ with = 0.25 and = 0.05.

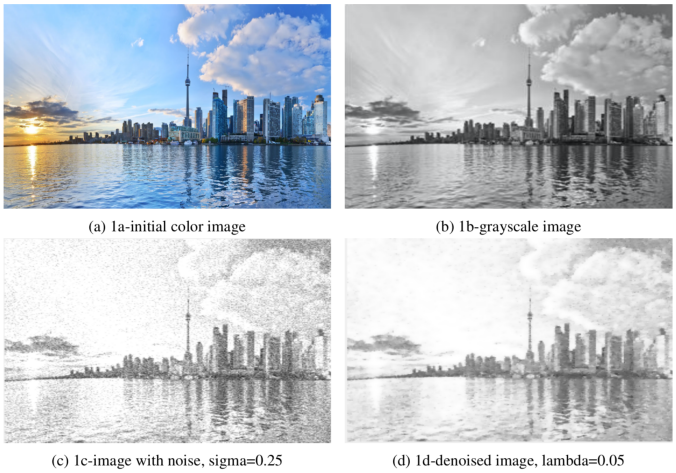

(a) 1a-initial color image (b) 1b-grayscale image

(c) 1c-image with noise, sigma=0.25 (d) 1d-denoised image, lambda=0.05

Fig. 5. Chambolle's projection algorithm with fixed λ. [26]

The second group(Fig.6) of images show the results of the

Chambolle's projection algorithm with optimal λ with $= 0.2$, and $= 0.1$.

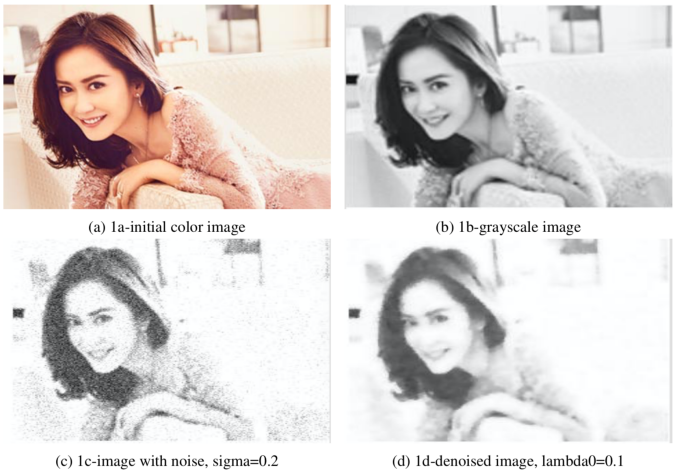

(a) 1a-initial color image (b) 1b-grayscale image

(c) 1c-image with noise, sigma=0.2 (d) 1d-denoised image, lambda0=0.1

Fig. 6. Chambolle's projection algorithm with optimal λ. [26]

V. CONCLUSION

The applications of image denoising have been widely used in people's everyday lives, and the search for efficient image denoising algorithms is still a challenge problem for researchers.

In this article, we investigated into image denoising problems via convex optimization, and analyzed three state of the art methods : Multi-Objective Low-Rank and Sparse Model, Transforms based Tensor Robust PCA and Chambolle's Dual Method both from theoretical perspective and numerical results. Since different noises may require different denoising methods, the analysis can be useful in exploring new image denoising methods.

This project not only significantly improved our understanding and skills in convex optimization, but also ignited our passion in image denoising and computer vision.

VI. POSSIBLE FUTURE WORKS

As we researched on image denoising problems, we found that one difficulty lies in how to extract the data presentation, in which machine learning and deep learning methods has achieved great performance. In this sense, machine learning and deep learning methods might be more widely exploited in solving image denoising problems. But one disadvantage of deep learning is that there may not existing so many image pairs in real life to train the deep learning models. Therefore, deep learning-related methods may not be sufficiently effective. In this aspect, exploring more advanced methods that do no need so many image pairs for training will be a hot direction of image denosing.

But there still exist other obstacles in real image denosing, one of which is that the real noise is much more complex and diverse than that in experiments. In this situation, the thorough evaluation of a denoiser will be a hard task. In in-camera pipeline, there are components like color demosaicing, color transform, compression, etc that may lead to noised images. Therefore, how to handling these external and internal conditions is also another topic of image denosing.

REFERENCES

[1] S. Anwar, C. P. Huynh, F. Porikli, T. Kim, S. Zafeiriou, G. Brostow, and K. Mikolajczyk, "Combined internal and external category-specific image denoising." in *BMVC*, 2017.

[2] F. Chen, L. Zhang, and H. Yu, "External patch prior guided internal clustering for image denoising," in *Proceedings of the IEEE international conference on computer vision*, 2015, pp. 603–611.

[3] J. Xu, L. Zhang, W. Zuo, D. Zhang, and X. Feng, "Patch group based nonlocal self-similarity prior learning for image denoising," in *Proceedings of the IEEE international conference on computer vision*, 2015, pp. 244–252.

[4] Y. Zhang, X. Tian, and P. Ren, "An adaptive bilateral filter based framework for image denoising," *Neurocomputing*, vol. 140, pp. 299–316, 2014.

[5] E. J. Balster, Y. F. Zheng, and R. L. Ewing, "Feature-based wavelet shrinkage algorithm for image denoising," *IEEE transactions on image processing*, vol. 14, no. 12, pp. 2024–2039, 2005.

[6] Z. Zha, X. Yuan, J. Zhou, C. Zhu, and B. Wen, "Image restoration via simultaneous nonlocal self-similarity priors," *IEEE Transactions on Image Processing*, vol. 29, pp. 8561–8576, 2020.

[7] Y. Wan, A. Ma, W. He, and Y. Zhong, "Accurate multi-objective low-rank and sparse model for hyperspectral image denoising method," *IEEE Transactions on Evolutionary Computation*, 2021.

[8] W. Dong, F. Fu, G. Shi, X. Cao, J. Wu, G. Li, and X. Li, "Hyperspectral image super-resolution via non-negative structured sparse representation," *IEEE Transactions on Image Processing*, vol. 25, no. 5, pp. 2337–2352, 2016.

[9] D. Chen, S. Sun, C. Zhang, Y. Chen, and D. Xue, "Fractional-order tv-l2 model for image denoising," *Central European Journal of Physics*, vol. 11, no. 10, pp. 1414–1422, 2013.

[10] M. Maggioni, V. Katkovnik, K. Egiazarian, and A. Foi, "Nonlocal transform-domain filter for volumetric data denoising and reconstruction," *IEEE transactions on image processing*, vol. 22, no. 1, pp. 119–133, 2012.

[11] H. Zhang, W. He, L. Zhang, H. Shen, and Q. Yuan, "Hyperspectral image restoration using low-rank matrix recovery," *IEEE transactions on geoscience and remote sensing*, vol. 52, no. 8, pp. 4729–4743, 2013.

[12] W. He, H. Zhang, L. Zhang, and H. Shen, "Total-variation-regularized low-rank matrix factorization for hyperspectral image restoration," *IEEE transactions on geoscience and remote sensing*, vol. 54, no. 1, pp. 178–188, 2015.

[13] H. K. Aggarwal and A. Majumdar, "Hyperspectral image denoising using spatio-spectral total variation," *IEEE Geoscience and Remote Sensing Letters*, vol. 13, no. 3, pp. 442–446, 2016.

[14] L. Zhuang and J. M. Bioucas-Dias, "Fast hyperspectral image denoising based on low rank and sparse representations," in *2016 IEEE International Geoscience and Remote Sensing Symposium (IGARSS)*. IEEE, 2016, pp. 1847–1850.

[15] Y. Wang, J. Peng, Q. Zhao, Y. Leung, X.-L. Zhao, and D. Meng, "Hyperspectral image restoration via total variation regularized low-rank tensor decomposition," *IEEE Journal of Selected Topics in Applied Earth Observations and Remote Sensing*, vol. 11, no. 4, pp. 1227–1243, 2017.

[16] C. Cao, J. Yu, C. Zhou, K. Hu, F. Xiao, and X. Gao, "Hyperspectral image denoising via subspace-based nonlocal low-rank and sparse factorization," *IEEE Journal of Selected Topics in Applied Earth Observations and Remote Sensing*, vol. 12, no. 3, pp. 973–988, 2019.

[17] B. Rasti, P. Ghamisi, and J. A. Benediktsson, "Hyperspectral mixed gaussian and sparse noise reduction," *IEEE Geoscience and Remote Sensing Letters*, vol. 17, no. 3, pp. 474–478, 2019.

[18] W. He, H. Zhang, H. Shen, and L. Zhang, "Hyperspectral image denoising using local low-rank matrix recovery and global spatial–spectral total variation," *IEEE Journal of Selected Topics in Applied Earth Observations and Remote Sensing*, vol. 11, no. 3, pp. 713–729, 2018.

[19] C. Lu, "Transforms based tensor robust pca: Corrupted low-rank tensors recovery via convex optimization," in *Proceedings of the IEEE/CVF International Conference on Computer Vision*, 2021, pp. 1145–1152.

[20] D. Martin, C. Fowlkes, D. Tal, and J. Malik, "A database of human segmented natural images and its application to evaluating segmentation algorithms and measuring ecological statistics," in *Proceedings Eighth IEEE International Conference on Computer Vision. ICCV 2001*, vol. 2. IEEE, 2001, pp. 416–423.

[21] E. J. Candès, X. Li, Y. Ma, and J. Wright, "Robust principal component analysis?" *Journal of the ACM (JACM)*, vol. 58, no. 3, pp. 1–37, 2011.

[22] B. Huang, C. Mu, h. D. Goldfarb, and J. Wright, "Provable models for robust low-rank tensor completion," *Pacific Journal of Optimization*, vol. 11, no. 2, pp. 339–364, 2015.

[23] C. Lu, J. Feng, Y. Chen, W. Liu, Z. Lin, and S. Yan, "Tensor robust principal component analysis with a new tensor nuclear norm," *IEEE transactions on pattern analysis and machine intelligence*, vol. 42, no. 4, pp. 925–938, 2019.

[24] L. I. Rudin, S. Osher, and E. Fatemi, "Nonlinear total variation based noise removal algorithms," *Physica D: nonlinear phenomena*, vol. 60, no. 1-4, pp. 259–268, 1992.

[25] A. Chambolle, "An algorithm for total variation minimization and applications," *Journal of Mathematical imaging and vision*, vol. 20, no. 1, pp. 89–97, 2004.

[26] X. C. Zhang, "Application of convex optimization in grayscale image denoising using chambolle's projection mehtod, and the method's generalization to rotational objects," 2016.